Lec 4

1.1 **Electroceramics**

Electroceramics are ceramic materials that are characterised by unique electrical properties, in addition to their mechanical and thermal properties, which make them suitable for use in the electrical and electronics industries [1].

many different properties were discovered and manipulated for a wide range of applications. As a result, various subclasses of electroceramics have been developed in conjunction with the growth of new technologies [2]. For example, functional electroceramic materials include ferroelectrics (high dielectric permittivity capacitors), piezoelectrics (sound and ultrasound transducers) and pyroelectrics (thermal sensors). Figure 2-1 illustrates the classification of electroceramics according to their functionality, which is dependent on crystal structure [3].

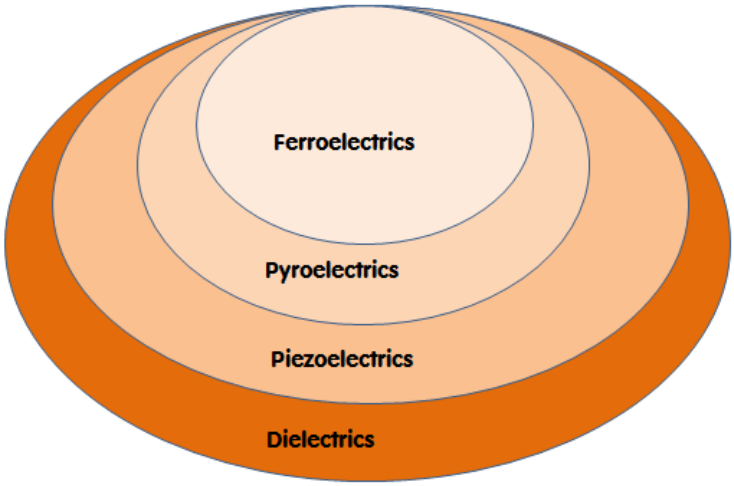

Figure 2-1. Classification of dielectric materials [3].

1.1.1 **Dielectrics**

Dielectric materials are characterised by high electrical resistivity, which enables them to be used as electrical insulators. An ideal dielectric does not conduct electric charge when placed in an electric field, E. Instead, it becomes polarized due to the separation of positive and negative charges over a certain distance, creating a dipole moment. In other words, the dielectric possesses a polarisation, *P*, which is defined as the net dipole moment (*p*) per unit volume (*V*). *P* is measured in units of C m / m^3 = C m^{-2}. There are four fundamental polarization mechanisms including atomic or electronic, ionic, dipolar and space charge or diffusional, as illustrated in Figure 2-2[2]. Each mechanism has its

own characteristic response time, which leads to the schematic frequency-dependence of dielectric permittivity illustrated in Figure 2-4.

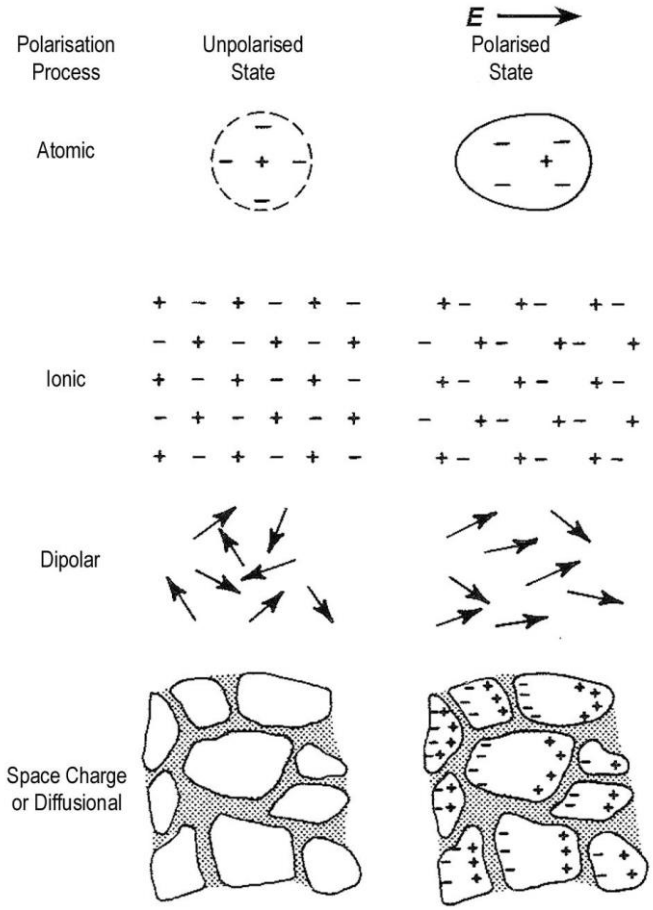

Figure 2-2. Schematic representation of different mechanism of polarization **[2]**.

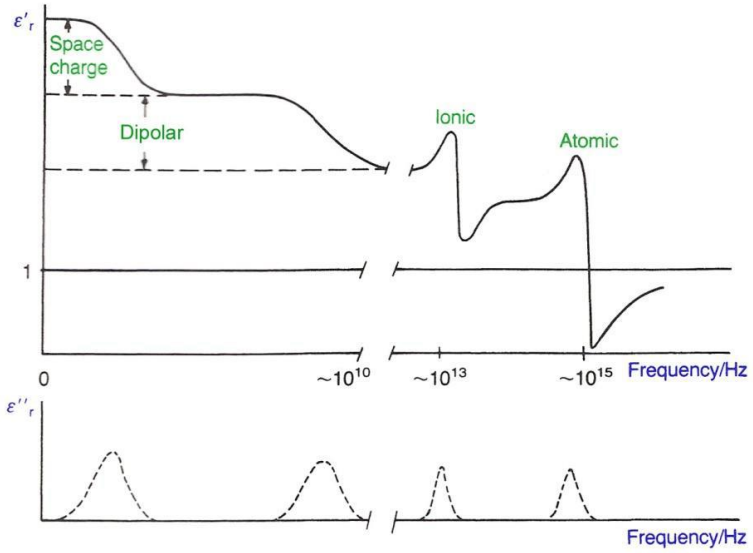

Figure 2-3. Schematic illustration of variations in dielectric constant ε_r' and loss ε_r'' as a function of frequency **[2]**.

1.1.1.1 **Relative permittivity and capacitance**

The properties of most concern for the dielectrics are the dielectric constant or relative permittivity, dielectric loss and dielectric strength. However, it is necessary first to clarify how polarization is measured and what is the relationship between the polarisation and the dielectric properties.

Consider two conductive parallel plates (i.e. a capacitor) of area, *A*, separated by a distance, d, in vacuum, as shown in Figure 2-4(a). When an electric field is applied, the charges $\pm Q$ will be distributed uniformly over opposite surfaces of the plates.

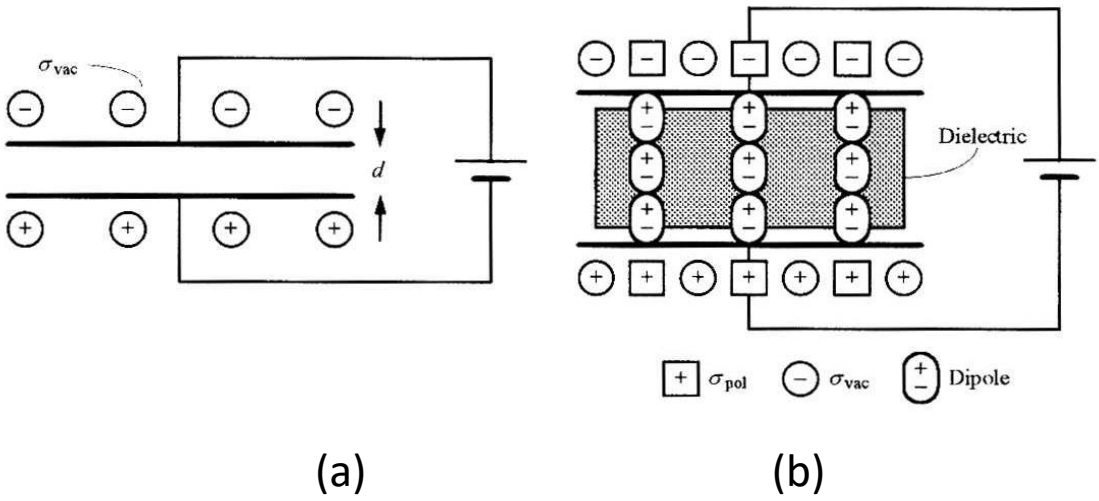

Figure 2-4. Schematic diagrams of a parallel-plate capacitor showing how charge can be stored on capacitor plates in (a) vacuum and (b) when a dielectric is placed between the plates [4].

Increasing the applied voltage, *V*, causes a linear increase in the stored charge, *Q*, according to equation 2-2, as shown in Figure 2-5.

$$Q = \boldsymbol{C}.\boldsymbol{V} \tag{2-1}$$

The slope of the *Q* versus *V* curve is the capacitance, C_o, (free space) of the parallel plates in vacuum, given by:

$$\boldsymbol{C_o} = \frac{\boldsymbol{\varepsilon_o}\,.\,\boldsymbol{A}}{\boldsymbol{d}} \tag{2-2}$$

where ε_o is the permittivity of free space, equal to 8.85×10^{-12} F m^{-1}.

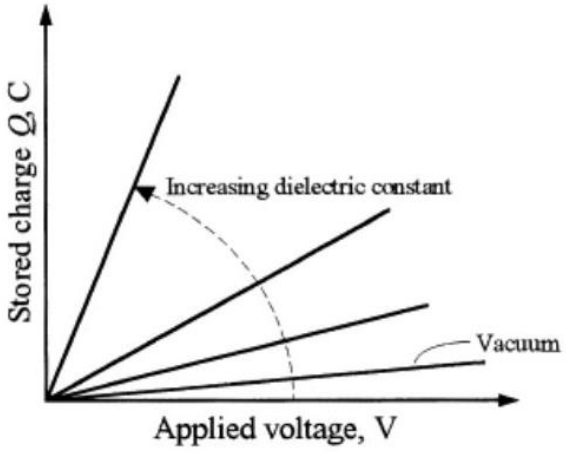

Figure 2-5. Functional dependence of *Q* on applied voltage. The gradient of each line is equal to the capacitance, which is proportional to the dielectric constant of the material [4].

If a dielectric is placed between the plates, as shown in Figure 2-4(b) and an electric field is applied, the stored charge will increase as seen in Figure 2-5, where the slope of the *Q*-*V* curve is larger than that for a vacuum.

In other words, Eq. (2.4) is modified as:

$$\boldsymbol{C = \frac{\varepsilon \,.\, A}{d}} \tag{2-3}$$

where ε is the *permittivity* of the dielectric between the plates.

The *relative permittivity*, or *dielectric constant*, of a material, ε_r, is defined as the ratio between the permittivity of a material to that of vacuum. Hence, it is a dimensionless parameter. Since ε is always greater than ε_o, the minimum value for ε_r is 1.

$$\boldsymbol{\varepsilon_r = \frac{\varepsilon}{\varepsilon_o}} \tag{2-4}$$

1.1.1.2 **Dielectric loss**

Another important property of a dielectric is the dielectric loss of a material under an alternating field. When an alternating voltage is applied across an ideal dielectric, the phase of current , *I,* through the capacitor would be ahead of the phase of voltage, *V,* by an angle of 90° as shown in Figure 2-6a.

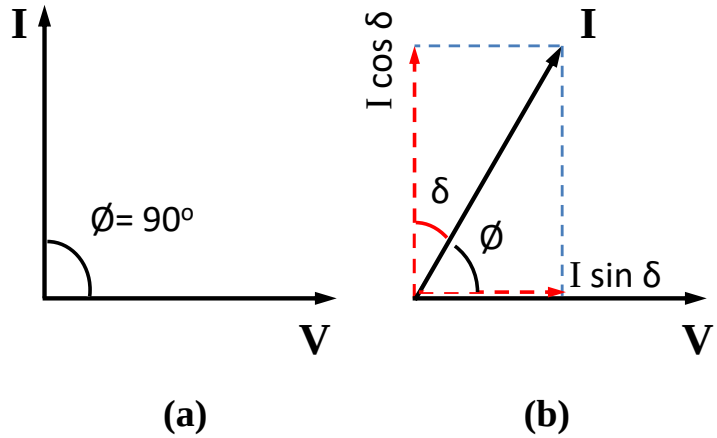

Figure 2-6. Representative diagram of (a) ideal dielectric and (b) real lossy dielectric , illustrating phase angle, ϕ, and loss angle, δ [4].

However, the phase angle, ϕ, differs from 90° in presence of a real lossy dielectric, where the polarization is no longer in phase with the applied voltage. In such a case, the resulting current leads the applied voltage by an angle, ϕ = 90° - δ as shown in Figure 2-6(b), where δ is known as the loss angle. The current can be factorized into two components; the *capacitive component* leads the applied voltage by an angle of 90° and the *resistive component* is in-phase with the applied voltage. The former is given by I cos δ and is denoted the *imaginary* component of current while the latter is given by I sin δ and is denoted the *real* component of current.

The quantity tan δ is a measure of power loss. It is commonly known as the *loss tangent*, or *dissipation factor*. It may be defined as the ratio of the imaginary component of dielectric constant, ε″, to the real component, ε', according to equation 2-9.

$$\tan \delta = \frac{\varepsilon''}{\varepsilon'} \qquad (2\text{-}5)$$

Lec 4

1.1.1.3 **Dielectric Breakdown (dielectric strength)**

When a dielectric is subjected to an ever-increasing electric field, at some points a short circuit develops across it. **Dielectric breakdown** is defined as the voltage gradient or electric field sufficient to cause the short circuit. This phenomenon depends on many factors, such as sample thickness, temperature, electrode composition and shape, and porosity.

In ceramics, there are two basic types of breakdown: intrinsic and thermal [29,52].

• *Intrinsic breakdown:* In this mechanism, electrons in the conduction band are accelerated to such a point that they start to ionize lattice ions. As more ions are ionized and the number of free electrons increases, an avalanche effect is created. Clearly, the higher the electric field applied, the faster the electrons will be accelerated and the more likely this breakdown mechanism will be.

• *Thermal breakdown:* The criterion for thermal breakdown is that the rate of heat generation in the dielectric, as a result of losses, must be greater than the rate of heat removal from the sample. Whenever this condition occurs the dielectric will heat up, which in turn will increase its conductivity, which causes further heating, etc. This is termed *thermal breakdown* or *thermal runaway* [29].

$$\text{Dielectric Strength} = \frac{V_{av}}{h}$$

As:

V_{av}: Rate of breakdown voltage (kV)

h : Thickness (mm)

Lec 4

1.1.2 **Ferroelectrics**

Ferroelectrics (FEs) are ceramic materials that possess spontaneous electric polarisation even in the absence of external electric fields due to the non-centrosymmetric arrangement of the ions and their electrons in these materials. The direction of spontaneous polarization can be reoriented by an electric field. This phenomenon is called *ferroelectricity*.

It is necessary to clarify the non-centrosymmetric nature of crystal structures in order to understand the origins of ferroelectricity and its relation to piezoelectricity and pyroelectricity that will be discussed in the following sections.

In crystallography, the symmetry about a point in space, e.g. the central point of a unit cell, can be defined using elements such as (1) a centre of symmetry, (2) axes of rotation, (3) mirror planes, and (4) combinations of these. Based on these elements of symmetry, the seven basic crystal systems, described in section 2.1 below, are classified into 32 point groups. Of these, just 21 are non-centrosymmetric point groups, as shown in Figure 2-7 [5]. This feature is necessary for a crystal to exhibit the phenomena of ferroelectricity, piezoelectricity and pyroelectricity [6] .

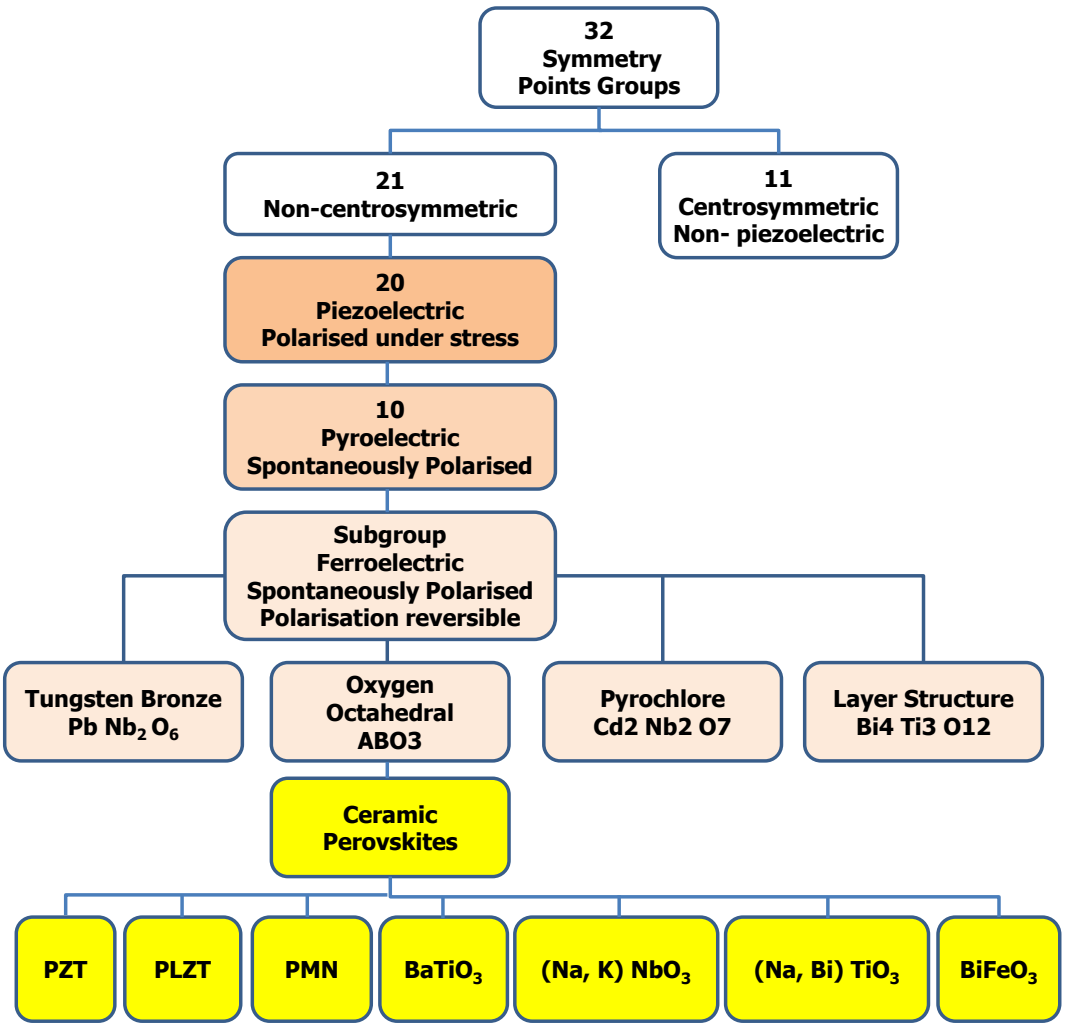

Figure 2-7. Classification of crystals based on symmetry, showing the interrelationship of ferroelectrics and subgroups and their common crystal structures with examples **[5]**.

1.1.2.1 **Crystal structure**

A *crystal* is a solid object that consists of a periodic arrangement of atoms in three dimensions. The smallest repeating volume of the ordered arrangement of atoms is called the *unit cell*. The positions that are occupied by the atoms within the unit cell are called *lattice points*; the geometric arrangement of these can be described by Bravais lattices. The main points are located at the corners of the unit cell and called *Primitive or simple (P)*. Additionally, three points are potentially occupied, which are located at the centre, *body-centred (I)*, one face, *base-centred (C*), or at all faces of the unit cell, *face-centred (F)* [6].

Furthermore, the unit cell is characterized by three lattice constants a, b, c (the lengths of the basis vectors) and by the three angles α, β, γ which separate these vectors from one another.

Based on these parameters and Bravais lattices, there are seven crystal systems and fourteen crystal types as listed in the Table 2-1.

Table 2-1. Crystal systems with crystallographic parameters and Bravais lattices [6].

	Crystal System	Bravais Lattice	Unit cell lattice constants and angles	Order of symmetry
1	Triclinic	1- Primitive (P)	$a \neq b \neq c$ $\alpha \neq \beta \neq \gamma$	Increasing symmetric
2	Monoclinic	1- Primitive (P) 2- Base-Centered (C)	$a \neq b \neq c$ $\alpha = \gamma = 90° \neq \beta$	
3	Orthorhombic	1- Primitive (P) 2- Base-Centered (C) 3- Body-Centered (I) 4- Face-Centered (F)	$a \neq b \neq c$ $\alpha = \beta = \gamma = 90°$	
4	Rhombohedral or Trigonal	1- Primitive (P)	$a = b = c$ $\alpha =$ $\beta = \gamma < 120 \neq 90°$	
5	Tetragonal	1- Primitive (P) 1- Body-Centered (I)	$a = b \neq c$ $\alpha = \beta = \gamma = 90°$	
6	Hexagonal	2- Primitive (P)	$a = b \neq c$ $\alpha = \beta = 90°, \gamma = 120°$	
7	Cubic	1- Primitive (P) 2- Body-Centered (I) 3- Face-Centered (F)	$a = b = c$ $\alpha = \beta = \gamma = 90°$	

1.1.2.2 **The perovskite structure**

The name *perovskite* comes from the mineral $CaTiO_3$. Barium titanate, $BaTiO_3$, and lead zirconate titanate, $Pb(Zr_{1-x}Ti_x)O_3$, represent some of the most common ceramic compounds that have a perovskite structure [7]. This structure is a binary oxide compound with the general formula ABO_3 (where A and B are different cations) as shown in Figure 2-8. The larger A cation, together with oxygen anions, make up a face centred cubic (FCC) lattice (coordinated with 12 oxygen ions) and the smaller B cation occupies the octahedral interstitial sites in the array (coordinated with 6 oxygen ions). The structure can also be viewed as a network of corner-linked oxygen octahedra [8].

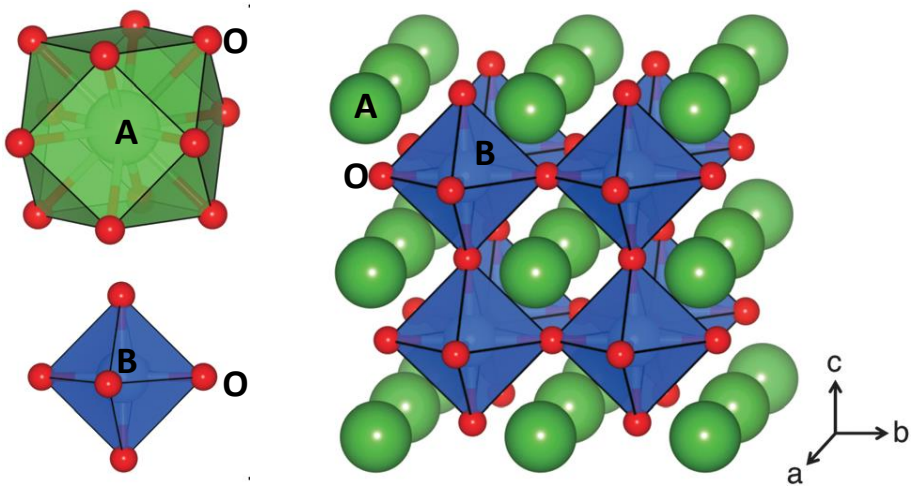

Figure 2-8. Prototypical ABO_3 perovskite structure, emphasizing the dodecahedral interstice with the A-ion in the center (AO_{12}) and the octahedral interstice with the B-ion in the centre (BO_6) [9].

The perovskite structure supports a wide range of ions on the A- and B- sites. The valence of the A-site cations can range from +1 to +3 (e.g. Ba^{2+}), while for the B-site cations it can range from +2 to +6 (e.g. Ti^{4+}) [7]. The substitution with different ions causes a distortion in the prototype perovskite structure as a result of mismatch in ionic size between the A- and B- sites. Therefore, Goldschmidt proposed a geometrical relationship based on the ionic radii of the ions occupying these sites, described as a *tolerance factor*, *t*, to estimate this distortion and indicate the stability of a compound [10]. The tolerance factor is given as:

$$t = \frac{R_A + R_O}{\sqrt{2}(R_B + R_O)} \quad (2\text{-}6)$$

where R_A, R_B, and R_O are the ionic radii of the A-site, B-site, and oxide ions, respectively. Compounds have been observed to form in the perovskite structure for *t* values in the range $0.88 \leq t \leq 1.09$. Thus, it is evident that the perovskite structure supports a wide range of ion substitutions, which permits doping and/or modification to

1.1.2.3 **Ferroelectric domains and hysteresis**

As reported above, ferroelectric materials are characterised by spontaneous polarisation, which results from aligned dipole moments in the crystal. The regions of uniformly oriented dipoles are called *ferroelectric domains*; these are separated by boundaries, referred to as *domain walls*. In a typical polycrystalline ferroelectric, the domains are

randomly oriented. In such a state, the differently-oriented regions of spontaneous polarization cancel each other out since the polarisation is a vector quantity.

This randomly-oriented domains can be aligned towards the same direction by subjecting the material to a strong electric field. This process is called *poling* and can be characterised by a P-E hysteresis loop, as shown in Figure 2-9; this illustrates the relationship between the polarisation and the electric field and is a key property of a given ferroelectric material [11].

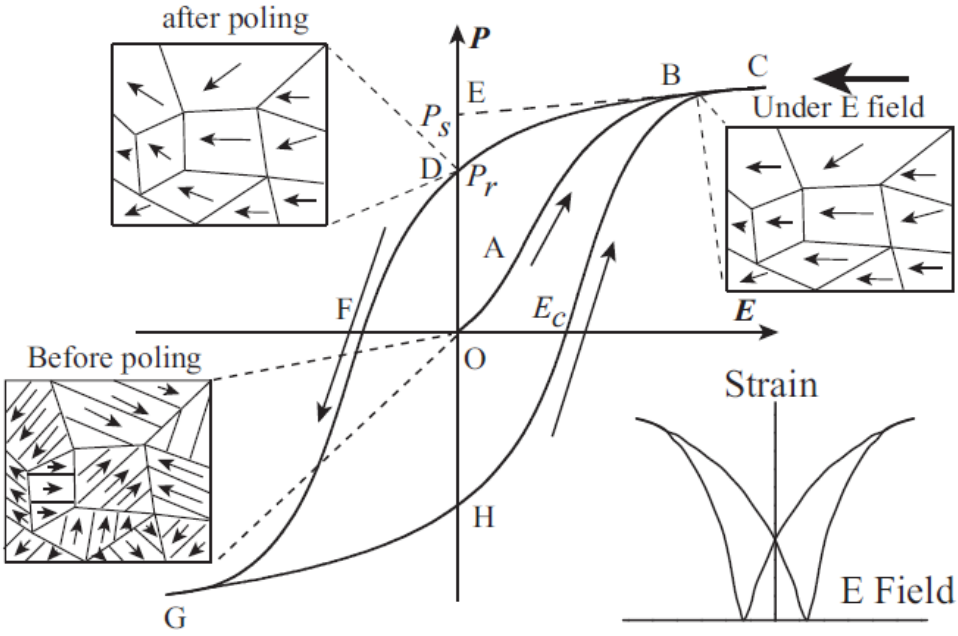

Figure 2-9. Representative electric field-induced polarization hysteresis loop of FEs and strain-electric field curve **[11]**.

1.1.2.4 **Curie- Weiss law**

Ferroelectric materials lose their spontaneous polarisation at temperatures above a specific point, called the *Curie temperature*, T_C. In other words, the material transforms from a ferroelectric to paraelectric state, which is characterised by high crystal symmetry due to the structural phase transition and behaves as a linear dielectric showing a straight line in P-E relationship instead of a hysteresis loop [12].

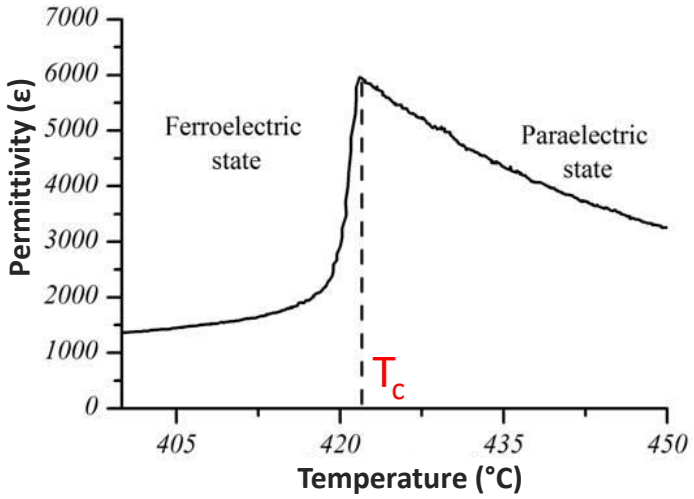

Figure 2-10. Temperature-dependence of permittivity for a ferroelectric material [13].

1.1.2.5 **Relaxor Ferroelectrics**

Relaxor ferroelectric materials (RFs) are classified as ferroelectrics, but display additional or different functional behaviour in comparison with *normal ferroelectrics* (NFs). They are characterised by random occupation of one or more ions in the equivalent site within the unit cell [14]. This disordered distribution generates unique structural and functional properties [15]. Figure 2-11 illustrates the differences in the characteristic features of NFs and RFs.

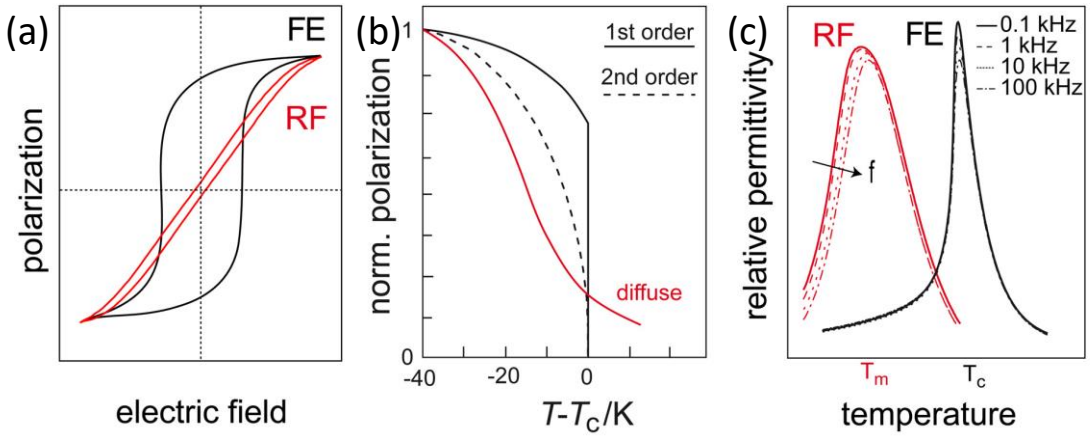

Figure 2-11. Schematic illustration of relaxor (RF) and normal ferroelectrics (NF) (a) P-E hysteresis loop (b) thermal depolarisation and (c) relative permittivity [16, 17].

In terms of the P-E hysteresis, NFs exhibit a rectangular P-E loop with strong remanent polarization P_r. In contrast, RFs show a slim loop with low P_r and E_c values, as shown in Figure 2-11(a).

Lec 4

1.1.3 **Piezoelectricity in ferroelectrics**

Piezoelectricity is a term used to describe two effects in the subclass of ferroelectrics called piezoelectrics, which are the ability to generate electric polarisation under an applied mechanical stress or mechanical strain under an applied electric field. They are referred to as the *direct piezoelectric effect* or *converse effect*, respectively as shown in Figure 2-12 [18]. 20 out of the 21 non-centrosymmetric point groups exhibit piezoelectricity as illustrated in Figure 2-7.

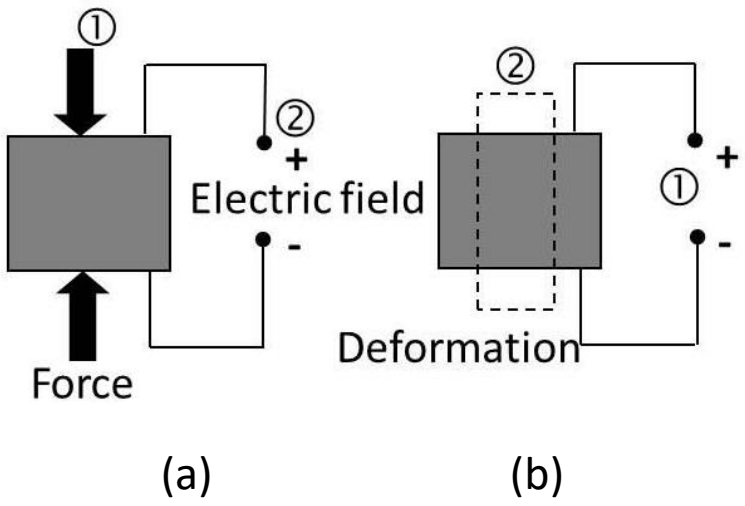

Figure 2-12. Illustration of (a) direct and (b) converse piezoelectric effects **[2]**.

The relationships between the mechanical and electrical parameters for both effects are given by the following equations:

$$\boldsymbol{D_i = d_{ij}X_j} \quad \text{direct piezoelectric effect} \tag{2-7}$$

$$\boldsymbol{x_i = d_{ij}E_j} \quad \text{indirect } \textit{(converse)} \text{ piezoelectric effect} \tag{2-8}$$

Here, X is the mechanical stress, x is the field-induced strain, E is the electric field, and D is the dielectric displacement. D is related to the polarization P by $D = \varepsilon_o E + P$. The proportionality factor d_{ij} is denoted the *piezoelectric charge* or *strain* coefficient. The indices i and j refer to the directions in which X, x, E and D are applied or generated. Of these, 3 indicates the polarization direction, 1 and 2 are directions perpendicular to 3 and each other, as shown in Figure 2-13.

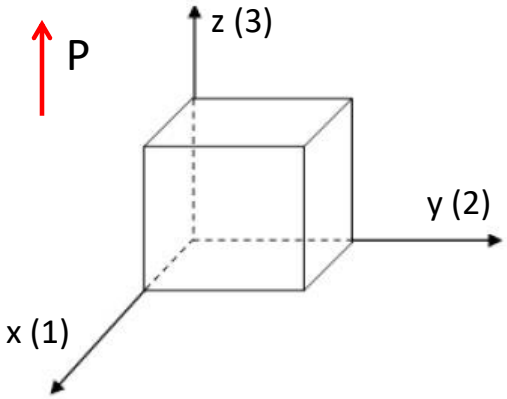

Figure 2-13 labelling of reference axes and planes for piezoceramics.

The longitudinal piezoelectric cefficient (d_{33}) is often reported, which relates the mechanical stress and electrical displacement (or mechanical strain and electric field strength) components in the direction of the macroscopic average polarization. It is an important figure of merit for the piezoelectric effect and especially important for sensors.

1.1.4 **Pyroelectricity in ferroelectrics**

Pyroelectricity is defined as a phenomenon in which a temporary voltage is excited due to a polar, pyroelectric material being either heated up or cooled down [2]. When a pyroelectric material is heated, the internal electric dipoles change in magnitude or undergo re-orientation to produce an overall change in polarisation and charge displacement. There are 10 crystal classes out of 21 non-centrosymmetric point groups that are designated as pyroelectric [19].

1.2 **Applications of Ferroelectric materials**

The discovery of characteristic features of ferroelectrics and related materials including piezoelectrics and pyroelectrics has led to the development of new materials that have numerous commercial uses. These cover a wide range of applications for military and civilian use including those in our workplaces, homes, and automobiles. Examples of

ferroelectrics that have high dielectric constant with low loss are memory storage and high power, high energy capacitors for hybrid vehicles, ferroelectric thin-film memories and thin-film capacitors.

In term of piezoelectrics, they are well known as transducers due to their ability to transform the energy from one form into another, these can be categorised into piezo spark generators, sensors, actuators, and transducers. The categories cover many piezoelectric devices which can be classified into eleven types such as ultrasonic motors, actuators, Langevin actuators, piezoelectric transformers, resonators, transducers, piezoelectric generators including energy harvesters, sonars for military and civilian use, piezoelectric sensors and accelerators, acoustic devices, etc. An estimation of the individual market shares of these devices in 2017 was reported by Hong [20]. It was considered that actuators constitute the largest portion, around 32%.

On the other hand, pyroelectrics are utilised for detection of infrared (IR) radiation, thermal imaging, fire detection and motion sensing etc. [2].

1.3 **Ferroelectric materials**

1.3.1 **Lead-based ferroelectric materials**

The most popular lead-based ferroelectric and piezoelectric material in industrial applications is lead zirconate titanate (PZT) ceramic. It was discovered by Sawaguchi et al. around 1952 and still represents an important ferroelectric material [21, 22]. This is because the PZT compositions possess high piezoelectric and electromechanical coupling coefficients, exhibit high Curie point (T_C) which permits a high temperature of operation (above 200 $^{\circ}$C), can be easily poled, possess a wide range of dielectric constants, form solid solutions with many different constituents, thus allowing a wide range of achievable properties to meet the requirements of a specific application [23].

1.3.1.1 **Structure and phase transitions of PZT**

The PZT solid solution has a chemical formula of $Pb(Zr_{1-x}\ Ti_x)O_3$, where both Ti^{4+} and Zr^{4+} ions occupy the B-sites based on the general formula of perovskite structure, ABO_3. It is a solid solution of two perovskites, lead zirconate ($PbZrO_3$ or PZ) and lead titanate ($PbTiO_3$ or PT) as illustrated in Figure 2-14(a), which shows the phase diagram of PZT in the temperature range between 0 $^{\circ}$C to 500 $^{\circ}$C. This phase diagram is based on the works conducted by many authors [24].

Lec 4

At room temperature, three main regions can be observed in the PZ-PT pseudo-binary system. In the zirconium rich (Zr-rich) region, for $x \leq 0.05$, an antiferroelectric orthorhombic structure (A_O) is present, with space group *Pbam*. With increasing PT content (i.e. partial replacement of the Zr^{4+} ion with the Ti^{4+} ion), for $0.05 \leq x \leq 0.48$, the PZT compositions exhibit ferroelectric rhombohedral phase, including two types attributed to space groups *R3c* and *R3m*. Further increase of PT, for $0.48 \leq x \leq 1$, causes higher-level replacement of Zr^{4+} by Ti^{4+}. This Ti-rich region is characterised by a ferroelectric tetragonal phase, *P4mm*. In addition, another ferroelectric phase with monoclinic structure was observed at around x=0.48 [25, 26].

The highest level of the piezoelectric and dielectric properties can be obtained from PZT compositions that are located around x=0.48 as shown in Figure 2-14(b). This region is called the *morphotropic phase boundary* (MPB) region, where there is coexistence of two phases such as: rhombohedral+monoclinic or tetragonal+monoclinic. These outstanding properties result from an increased number of allowable domain states (six in ferroelectric tetragonal, eight in ferroelectric rhombohedral) [27].

With increasing temperature, both ferroelectric structures (rhombohedral and tetragonal phases) transform into cubic phase at the Curie temperature, while for a limited compositional range in the antiferroelectric orthorhombic phase (A_O) region there is a transformation at temperatures close to T_C into another antiferroelectric tetragonal phase (A_T) before the transformation to paraelectric cubic phase. Another interesting feature during heating is that the phase boundary between the tetragonal and rhombohedral phase (MPB) is nearly independent of temperature, unlike the phase boundary between the A_O and F_R which is more curved [23]. This leads to good stability of piezoelectric properties with temperature.

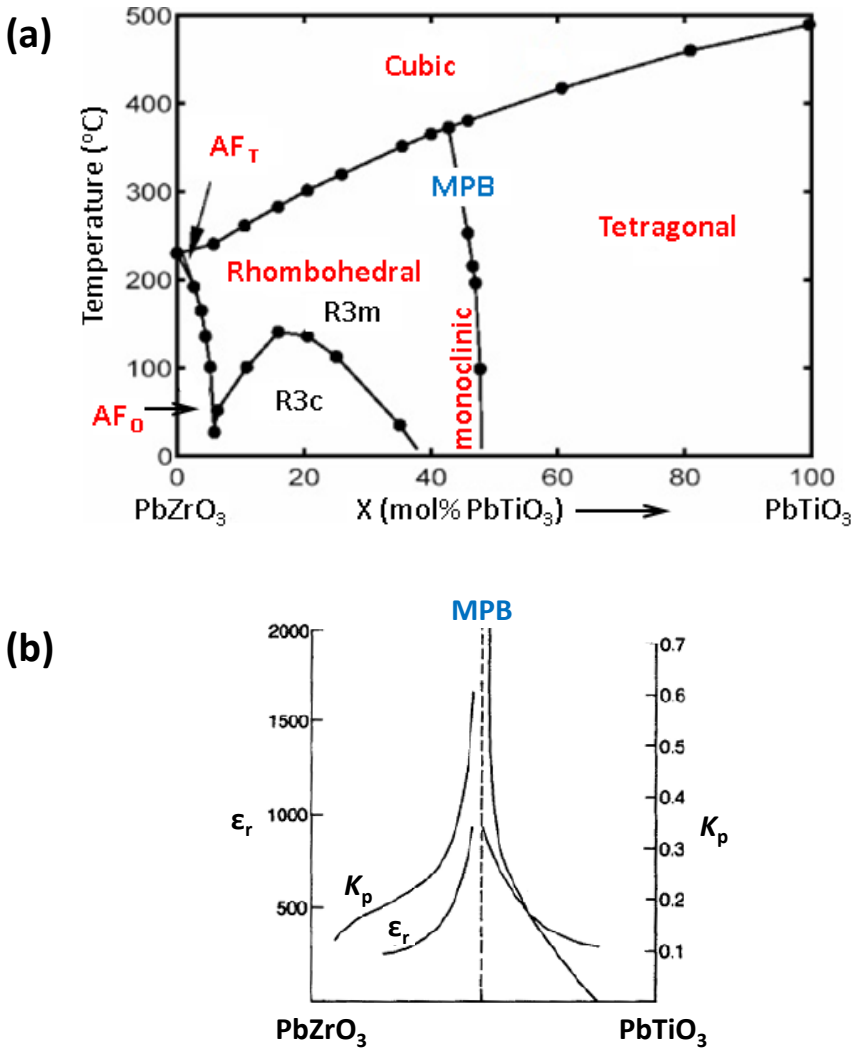

Figure 2-14. (a) Phase diagram of $PbZr_{(1-x)}Ti_xO_3$ (PZT) solid solution and (b) Coupling coefficient, k_p, and permittivity, ε_r, values across the PZT compositional range [24].

1.3.2 **Lead- free ferroelectric materials**

The high content of lead in PZT-based materials has created a strong desire in recent years to remove lead oxide as a component of piezoelectric ceramic products, due to its toxicity [28-31]. Therefore, it is necessary to develop new lead-free piezoelectric ceramics in order to substitute PZT in certain applications[20, 32]. The main candidate ceramic materials for this purpose are based on $BaTiO_3$ (BT), $(K_{0.5}Na_{0.5})NbO_3$ (KNN) and $(Bi_{0.5}Na_{0.5})TiO_3$ (BNT). Many investigations have been conducted on the synthesis and properties of these materials as pure compounds, modified by minor dopants, or in the form of solid solutions with other ABO_3 perovskites [29, 33]. In the present study, the focus will be on barium titanate (BT) and related materials.

Lec 4

1.3.2.1 **Barium titanate and related materials**

Barium titanate, $BaTiO_3$ (BT), was discovered before PZT, in 1941. It was found to have a crystal structure similar structure to that of the mineral perovskite ($CaTiO_3$), where Ba^{4+} and Ti^{4+} ions occupy the A- and B-sites, respectively [5]. To date, it has been used mainly as a capacitor dielectric due to its high dielectric constant and the ability to tailor the temperature-dependent dielectric properties by manipulation of the phase transformation temperatures through doping [34, 35]. It was found to exhibit ferroelectricity, and has been considered as the first polycrystalline material to possess this feature. However, it has relatively low piezoelectric properties and Curie temperature in comparison with PZT [36].

The lattice parameters of BT are affected by temperature, in common with other ferroelectric ceramics. It has a cubic structure above the Curie temperature (T_c) of approximately 120 ^oC, as illustrated in Figure 2-15 . As the temperature declines, this structure is distorted slightly to form a tetragonal ferroelectric phase with a dipole moment along the c-axis. Two further ferroelectric polymorphic transitions were identified, which are tetragonal to orthorhombic (T_{O-T}) or (T_1) at 0 ^oC, where the polarization axis is parallel to a face diagonal, and orthorhombic to rhombohedral (T_{R-O}) or (T_2) at -90 ^oC, where the polar axis is directed along a body diagonal (as indicated previously in section **Error! Reference source not found.**).

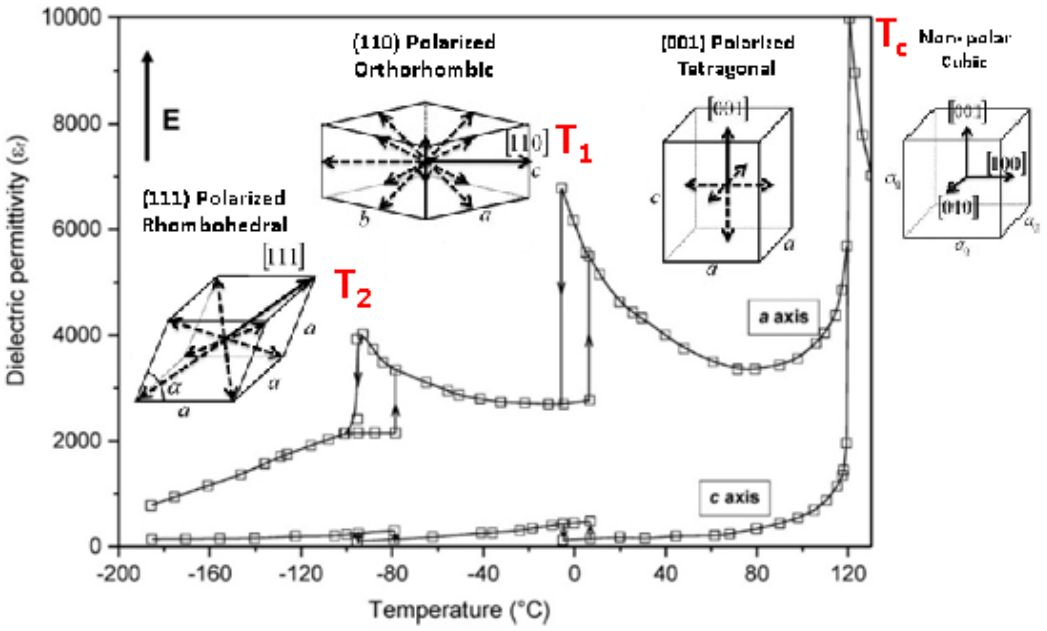

Figure 2-15. Temperature-dependence of dielectric permittivity and lattice parameters for $BaTiO_3$. Crystallographic nature of the polar axes are illustrated with reference to the cubic prototype perovskite structure [37].

2 References

[1] D. Richerson, " Modern Ceramic Engineering, Properties, Processing, and Use in Design," 1992.

[2] A. J. M. a. J. M. Herbert, *Electroceramics*. England: John Wiley & Sons, 2003.

[3] M. M. Blömker, "(Co)-Doping of lead-lree piezoceramics," PhD Thesis, Dem Fachbereich der Material- und Geowissenschaften Technische Universität Darmstadt, Darmstadt,, Darmstadt, 2016.

[4] M. W. Barsoum, *Fundamentals of ceramics*. CRC Press, 2002.

[5] G. H. Haertling, "Ferroelectric Ceramics: History and Technology," *J. Am. Ceram. Soc.*, vol. 82, no. 4, pp. 797–818 1999.

[6] K. C. Kao, *Dielectric phenomena in solids*. Elsevier Academic Press, 2004.

[7] Dal-Hyun and Do, "Investigation of ferroelectricity and piezoelectricity in ferroelectric thin film capacitors using synchrotron x-ray microdiffraction," PhD Thesis, PhD thesis, Metallurgical Engineering, University of Misconsin-Madison, 2006.

[8] B. Harari, "Development of high capacitance films for electrical energy storage using electrophoretic deposition of $BaTiO_3$ on ultrasonically etched Ni," MSC Thesis, MSC Thesis, Department of Mechanical and Materials Engineering, Queen's University, Kingston, Ontario, Canada, 2012.

[9] J. Young, P. Lalkiya, and J. M. Rondinelli, "Design of noncentrosymmetric perovskites from centric and acentric basic building units," *Journal of Materials Chemistry C*, vol. 4, no. 18, pp. 4016-4027, 2016.

[10] J. C. Frederick, "Strains and polarization developed during electric field-induced antiferroelectric to ferroelectric phase transformations in lead zirconate-based ceramics," MSC Thesis, MSC Thesis, Materials Science and Engineering, Iowa State University, 2010.

[11] L. Jin, F. Li, S. Zhang, and D. J. Green, "Decoding the Fingerprint of Ferroelectric Loops: Comprehension of the Material Properties and Structures," *Journal of The American Ceramic Society*, vol. 97, no. 1, pp. 1-27, 2014.

[12] M. Trainer, "Ferroelectrics and the Curie–Weiss law," *European Journal of Physics*, vol. 21, pp. 459–464, 2000.

[13] A. Ahmed, I. A. Goldthorpe, and A. K. Khandani, "Electrically tunable materials for microwave applications," *Applied Physics Reviews*, vol. 2, no. 1, p. 011302, 2015.

[14] R. A. Cowley, S. N. Gvasaliya, S. G. Lushnikov, B. Roessli, and G. M. Rotaru, "Relaxing with relaxors: a review of relaxor ferroelectrics," *Advances in Physics*, vol. 60, no. 2, pp. 229-327, 2011.

Lec 4

[15] C. Bharti, A. Dutta, and T. P. Sinha, "Structural and Ferroelectric Properties of Complex Perovskites $Pb_{(1-x)}Ba_x(Fe_{1/2}Ta_{1/2})O_3$(x = 0.00, 0.05, 0.1, 0.15)," *Ferroelectrics,* vol. 392, no. 1, pp. 20-32, 2009.

[16] R. Dittmer, "Lead-free piezoceramics –ergodic and nonergodic relaxor ferroelectrics based on bismuth sodium titanate," PhD thesis, PhD Thesis, University of Darmstadt, 2013.

[17] G. A. Samara, "The relaxational properties of compositionally disordered ABO_3 perovskites," *Journal of Physics: Condensed Matter,* vol. 15 pp. R367–R411, 2003.

[18] F. Dauchy, "Stress analysis, dielectric, piezoelectric, and ferroelectric properties of PZT thick films. fabrication of a 50MHz Tm-pMUT annular array.," PhD Thesis, PhD Thesis, School of Applied Science, Cranfield University, 2007.

[19] J. P. Sreekumar Uma, "Enhancement in Pyroelectric Properties of PZT-PVA Polymer Nanocomposites with Addition of PAA," *J. APPL. POLYM. SCI,* p. 41142 (1 of 8), 2014.

[20] C.-H. Hong *et al.*, "Lead-free piezoceramics – where to move on?," *Journal of Materiomics,* vol. 2, no. 1, pp. 1-24, 2016.

[21] G. H. Haertling, "Ferroelectric ceramics: history and technology," *Journal of the American Ceramic Society,* vol. 82, no. 4, pp. 797–818, 1999.

[22] P. K. Panda, "Review: environmental friendly lead-free piezoelectric materials," *Journal of Materials Science,* vol. 44, no. 19, pp. 5049-5062, 2009.

[23] L. Jin, "Broadband dielectric response in hard and soft PZT: understanding softening and hardening mechanisms," PhD Thesis, PhD Thesis, SwissFederal Institute of Technology-EPFL, Switzerland, 2011.

[24] B. Jaffe, W. Cook (Jr), and H. Jaffe, "Piezoelectric Ceramics," *Academic Press Inc,*

[25] B. Noheda *et al.*, "The monoclinic phase in PZT: New light on morphotropic phase boundaries," *AIP Conference Proceedings,* vol. 535, pp. 304-313, 2000.

[26] B. Noheda, D. E. Cox, G. Shirane, R. Guo, B. Jones, and L. E. Cross, "Stability of the monoclinic phase in the ferroelectric perovkite $PbZr_{1-x}Ti_xO_3$," *Physical Review B,* vol. 63, no. 1, pp. 014103-014103, 2001.

[27] C.-C. Chung, "Microstructural Evolution in Lead Zirconate Titanate (PZT) Piezoelectric Ceramics," PhD Thesis, PhD Thesis, University of Connecticut, 2014.

[28] W. Li, Z. Xu, R. Chu, P. Fu, and G. Zang, "High piezoelectric d_{33} coefficient in $(Ba_{1-x}Ca_x)(Ti_{0.98}Zr_{0.02})O_3$ lead-free ceramics with relative high Curie temperature," *Materials Letters,* vol. 64, no. 21, pp. 2325-2327, 2010.

[29] J.-F. Li, K. Wang, F.-Y. Zhu, L.-Q. Cheng, and F.-Z. Yao, "$(K,Na)NbO_3$-based lead-free piezoceramics: fundamental aspects, processing technologies, and remaining challenges," *Journal of The American Ceramic Society,* vol. 96, no. 12, pp. 3677-3696, 2013.

Lec 4

[30] J. Rödel, K. G. Webber, R. Dittmer, W. Jo, M. Kimura, and D. Damjanovic, "Transferring lead-free piezoelectric ceramics into application," *Journal of the European Ceramic Society,* vol. 35, no. 6, pp. 1659-1681, 2015.

[31] T. R. Shrout and S. J. Zhang, "Lead-free piezoelectric ceramics: alternatives for PZT?," *Journal of Electroceramics,* vol. 19, no. 1, pp. 113-126, 2007.

[32] P. K. Panda and B. Sahoo, "PZT to lead free piezo ceramics: a review," *Ferroelectrics,* vol. 474, no. 1, pp. 128-143, 2015.

[33] A. Maqbool *et al.*, "Structural, ferroelectric and field-induced strain response of Nb-modified $(Bi_{0.5}Na_{0.5})TiO_3$-$SrZrO_3$ lead-free ceramics," *Ferroelectrics,* vol. 488, no. 1, pp. 23-31, 2015.

[34] S.-W. Zhang, H. Zhang, B.-P. Zhang, and S. Yang, "Phase-transition behavior and piezoelectric properties of lead-free $(Ba_{0.95}Ca_{0.05})(Ti_{1-x}Zr_x)O_3$ ceramics," *Journal of Alloys and Compounds,* vol. 506, no. 1, pp. 131-135, 2010.

[35] G. K. Sahoo, "Synthesis and characterization of Zr and Ca Modified $BaTiO_3$ ferroelectric ceramics," PhD. Ph.D. thesis, PhD thesis, Department of Ceramic Engineering, National Institute of Technology, Odisha, India, Roll No: 509CR101, 2015.

[36] M. Acosta *et al.*, "$BaTiO_3$-based piezoelectrics: Fundamentals, current status, and perspectives," *Applied Physics Reviews,* vol. 4, no. 4, p. 041305, 2017.

[37] M. Villafuerte-Castrejón *et al.*, "Towards lead-free piezoceramics: facing a synthesis challenge," *Materials,* vol. 9, no. 1, p. 21, 2016.